Materials Research. 2021; 24(suppl. 1): e20210027
DOI: https://doi.org/10.1590/1980-5373-MR-2021-0027

Crystallization Kinetics and Structure Refinement of $CaTiO_3$ Glass-Ceramics Produced by Melt-Quenching Technique

Wagner da Silveira[a]*, *Wagner Costa Macedo*[a], *Gleyson Tadeu de Almeida Santos*[a], *Luis Fernando dos Santos*[a], *José Diego Fernandes*[a], *Kleper de Oliveira Rocha*[b], *Silvio Rainho Teixeira*[a]

[a]*Universidade Estadual Paulista (UNESP), Faculdade de Ciências e Tecnologia, Departamento de Física, 19060-900, Presidente Prudente, SP, Brasil.*
[b]*Universidade Estadual Paulista (UNESP), Faculdade de Ciências, Departamento de Química, 17033-360, Bauru, SP, Brasil.*

Received: January 12, 2021; Revised: March 25, 2021; Accepted: June 16, 2021

Glass-ceramic materials were obtained by heat treatment (960 ºC for 2, 4, and 6 hs) of glasses with $CaCO_3$ 47.50 wt%-TiO_2 23.75 wt%-SiO_2 23.75-Al_2O_3 5.00 wt% formulation produced by the melt-quenching technique (melting at 1650 ºC and subsequent annealing at 650 ºC). The materials' structural characterization and crystallization kinetics (Kissinger method) indicate the presence of $CaTiO_3$, $CaSiO_3$, and $CaTiSiO_5$ crystalline phases with activation energies 217, 281, and 446 kJ/mol, respectively. The structure refinement (Rietveld method) suggests metastability for the $CaSiO_3$ and $CaTiSiO_5$ phases as a function of the heat treatment time. The increase in time favors $CaTiO_3$ crystallization, from 62.97 wt%, in the 2 hs treated sample, to 79.21 wt%, in the 6 hs treated sample. EDS and microstructure analyses confirm the glass-ceramic production and indicate segregation of the $CaTiO_3$ phase for longer heat treatment times.

Keywords: Glass-ceramics, Melt-quenching Technique, $CaTiO_3$, Rietveld Method, Kissinger Method.

1. Introduction

Glass-ceramic materials are usually defined as materials with crystalline structures (0.5 to 99.5 wt%) embedded in a non-crystalline matrix (glassy phase)[1]. These materials were discovered accidentally in 1953 by S. D. Stookey and since then have been extensively studied. Research interest in these materials can be mainly attributed to their low apparent porosity, reduced thermal expansion coefficient and low water absorption, characteristics that can be associated with further desirable properties[2]. They also lend themselves to large scale production via any traditional technique aimed at the synthesis of glassy materials, such as the melt-quenching technique, thus being an attraction for the industrial sector[3].

As a result of their low water absorption and mechanical properties easily modified by their microstructure, glass-ceramic materials can be used in the construction sector, particularly in coatings. In these cases, glass-ceramic materials provide waterproof, mechanical resistance and considerable thermal insulation properties to the coated parts[4]. However, due to the emergence of new methods for the synthesis of glassy materials and new mathematical models (crystallization kinetics), novel glass-ceramic materials have emerged, which can be applied in multiple areas. Today, it is possible to obtain glass-ceramic materials with excellent mechanical properties from solid residues[5], develop bioactive glass-ceramics for coating implants[6,7], glass-ceramics that can be applied in photonics[8,9] or in energy storage devices with high thermal stability[10].

In the last decades there has been a considerable increase of demand for glass-ceramic materials aimed at electronic applications, with an emphasis on the development of perovskite glass-ceramics[11-14]. These are produced to obtain materials that provide both high dielectric constant or specific opto-electronic properties, and characteristics of most glass-ceramics, such as high mechanical resistance, impermeability and transparency. Classic perovskite glass-ceramics such as those based on $BaTiO_3$, $SrTiO_3$ and $PbTiO_3$, have properties similar to the respective bulk materials, however, these properties can be easily modified with the microstructure control of the obtained glass-ceramic[11].

A. Herczog[15] was able to synthesize $BaTiO_3$ glass-ceramics using the melt-quenching technique from the SiO_2-BaO-TiO_2-Al_2O_3-F system. In this case, three crystalline phases were observed, $BaTiO_3$, $BaAl_2Si_2O_8$ and $BaTiSiO_5$. Their percentages depend not only on the quantity of the precursors used but also on the temperature and the heat treatment time after obtaining the glasses. The author also points out the importance of understanding the crystallization kinetics of the studied system so that it is possible to develop new microstructures and predict the percentages of the crystalline phases present based on the thermal history of the studied material. Due to the lack of information in the literature, the objective of this work is to investigate the crystallization kinetics, structure refinement and microstructure analysis

*e-mail: wagnerdelages@hotmail.com

of $CaTiO_3$-based perovskite glass-ceramics obtained by the classic melt-quenching technique.

2. Literature Review

The first studies involving the synthesis of perovskite glass-ceramics were based on obtaining the $BaTiO_3$ phase crystallized in a glassy matrix of SiO_2, generally starting from the SiO_2-BaO-TiO_2-Al_2O_3 system[15-18]. These studies were motivated by known properties of the $BaTiO_3$ electroceramic, such as ferroelectricity, piezoelectricity, high dielectric constant and low loss factor[19,20], which could be enhanced by the high density and impermeability of glass-ceramics materials. Another motivation to study the $BaTiO_3$ glass-ceramic is the accessible melting temperature of the mixture of precursor oxides for the glass formation, which is around 1450 ºC – for the SiO_2 26 mol%-BaO-TiO_2 60 mol%-Al_2O_3 14 mol% system[21]. The success in obtaining this material spurred new research that culminated in the synthesis of other glassy and glass-ceramic materials of the perovskite type with important electrical and/or luminescent properties such as those based on $SrTiO_3$[22], $PbTiO_3$[23], $Li_{0.5}La_{0.5}TiO_3$[24] and $KZnF_3$[25].

Bulk $CaTiO_3$ electroceramics have been extensively studied in recent decades. Because of its particular electrical and luminescent properties, $CaTiO_3$ can be applied in electroluminescent devices[26], high performance capacitors[27], luminescent probes[28], biomedical materials[29], hydrogen production (water splitting)[30] and for the immobilization of radioactive waste[31]. However, its applications in the glass phase are poorly investigated and most studies focus on vitreous composites with added crystalline $CaTiO_3$ in their structure. Examples include the study of $MgTiO_3$-$CaTiO_3$ glass-ceramic compositions or the CaO-B_2O_3-SiO_2/$CaTiO_3$ system, both for LTCCs (Low Temperature Co-Fired Ceramics) applications[32,33]. One of the few systems that actually use this titanate as a component is the 55[(xPbO_{1-x}-CaO-TiO_2]-44 [2SiO_2-B_2O_3]-1Ge, which has been widely studied due to the possibility of improving the optical properties of borosilicate glasses[34].

Wollastonite ($CaSiO_3$) is another example of alkaline-earth perovskite widely used in the development of glass-ceramic materials. It has as its natural representative a characteristic white mineral and is widely used as a precursor (raw material) in inorganic syntheses, mainly those carried out by solid state reactions[35]. It has numerous applications and is frequently used in the glass-ceramic form, in coatings in civil construction or in biomedicine (bone implants)[36,37]. These well-known applications motivated research on several families of glass-ceramics with wollastonite as a component, such as $CaTiO_3$-$CaSiO_3$. These studies highlighted two main difficulties in preparing glasses with less than 65 mol% of $CaSiO_3$: rapid nucleation of $CaTiO_3$ crystals during quenching, and the need to reach in most cases 1600 ºC and above temperatures during the melting of the SiO_2-CaO-TiO_2 system[38].

To produce glassy and glass-ceramic materials using the melt-quenching technique it is necessary to analyze three characteristics of the studied system: (1) Composition: define and control the proposed composition, according to the desired properties for the final material; (2) Melting-point: check whether the melting-point of the precursor materials is accessible based on the available equipment and; (3) Crystallization: from the adopted cooling method, ensure that there is no crystallization of any phase (glassy materials) or ensure that there is a controlled crystallization of the desired phases (glass-ceramic materials). The high melting temperature and the rapid crystallization of $CaTiO_3$ are perhaps the main reasons why there is not much research on the production of $CaTiO_3$-based glass and glass-ceramics. In this context, this work aims to enrich the state of the art of this promising material.

3. Materials and Methods

3.1. Glass and Glass-Ceramics Production

The glassy material was prepared after calculating the precursor oxide formulation according to ternary phase diagram CaO-TiO_2-SiO_2, aiming at the region of greater stability for the $CaTiO_3$ phase[39,40]. $CaCO_3$ (Sigma-Aldrich, > 99.50%) – 47.50 wt%, TiO_2 (Sigma-Aldrich, > 99.50%) – 23.75 wt%, SiO_2 (Synth, 98%) – 23.75 wt% and Al_2O_3 (Alcoa, 85%) – 5.00 wt% were used as raw materials, and Al_2O_3 was used to increase the Ca ionic diffusion.

Precursor powders were mixed and grounded in an agate mortar for 2 hs, transferred to a high-density alumina crucible, and subjected to the melt-quenching technique[41]. The precursor materials were melted in a high-temperature oven (SERVIFOR) at 1650 ºC[38] with a holding time of 1 h at a heating rate of 10 ºC/min without atmosphere control. Then, the molten material was poured into a metallic mold (~ 6 cm in diameter), stamped, and immediately transferred to a low-temperature oven (mod. 3000, EDG) previously heated to 650 ºC, also without atmosphere control, where it remained for 1 h. This annealing was performed to minimize the rapid crystallization of $CaTiO_3$. The oven was turned off, and the sample naturally cooled to room temperature. The glass produced was named Ca Glass.

The glass-ceramic materials were obtained from the crystallization (nucleation + grain growth) of Ca Glass treated in a high-temperature oven at 960 ºC for 2, 4, and 6 hs. This temperature was chosen using the thermal analysis data of the Ca Glass – temperature just above the identified crystallization peak. The different holding times were studied to assess the stability of the crystallized phases.

3.2. Glass and Glass-Ceramics Characterization

Ca Glass was submitted to thermal analysis (SDT Q-600, TA Instruments) to determine the temperature to obtain the glass-ceramics and to develop the crystallization kinetics. For the thermal analysis, we used alumina crucibles, at an equilibrium temperature of 30 ºC, synthetic air atmosphere with a flow of 100 mL/min, heating rates of 10, 15, 20, 25, and 30 ºC/min and maximum temperature of 1200 ºC (an additional analysis was carried out up to 1300 ºC for the 10 ºC/min heating rate). Ca Glass was also subjected to X-ray fluorescence – XRF – (EDX7000, Shimadzu) to determine the real composition of the obtained glassy material. An Rh cathode was used as the primary source of radiation. The energy scan covered characteristic energies ranging from Na to U, in qualitative-quantitative mode, at room temperature. Biaxially-oriented polyester substrates

of poly(ethylene terephthalate) (boPET, Mylar®) were used. The observed energies were corrected to identify the most stable oxides found in nature.

The glassy and glass-ceramic samples were characterized by X-ray diffractometry – XRD – (XRD-6000, Shimadzu) at room temperature, using Cu $K_{\alpha 1}$ (λ = 1.5406 Å) and Cu $K_{\alpha 2}$ (λ = 1.5444 Å) radiation, 40 kV voltage, 30 mA current, scanning speed of 2º/min, divergence and reception slits of 1º, in continuous scanning mode, and 2θ angular range from 10º to 80º. The diffraction patterns were identified using the Powder Diffraction Files (PDF) of the JCPDS-ICDD (Joint Committee on Powder Diffraction Standards – International Center for Diffraction Data) database.

To complement the diffractogram analysis, the glass-ceramic samples (2, 4, and 6 hs) obtained through Ca Glass thermal treatment were also characterized by Raman scattering using a spectrometer (inVia, Renishaw), with a Leica microscope, 1800 lines/mm grid, and CCD detector. The scan was performed from 200 to 2000 cm^{-1}, using a 633 nm excitation laser (He-Ne source). The glass-ceramic sample treated during 6 hs was subjected to EDS (Energy-Dispersive X-ray Spectroscopy) analysis to verify the elemental distribution. The analysis used a scanning electron microscope – SEM (VEGA 3, TESCAN) in SE (Secondary Electrons) and BSE (Backscattered Electrons) modes. The sample was previously metalized with Au.

The glass-ceramic samples were sanded and polished using an alumina suspension for metallographic polishing (1 μm and 0.3 μm, respectively) to evaluate the microstructure. The samples were then chemically attacked using an HF solution (2% HF/98% distilled water) by immersion for 5 minutes. After drying, they were analyzed under an optical microscope (BX60M, Olympus) with a Leica EC3 camera attached (60x magnification).

3.3. Structure Refinement

The structure refinement used was based on the Rietveld Method (RM), a mathematical method developed by the dutch crystallographer H. Rietveld often used nowadays in the structure refinement of crystalline materials based on XRD data[42]. In general, the RM consists of adjusting a theoretical curve to the experimental diffractogram, using the least-squares approach to obtain the best approximations for structural parameters[43]. The RM was specifically used in this work to confirm the crystalline phases and to determine their percentages (in the glass-ceramic samples) without taking into account the non-crystalline phase.

The convergence parameters that make it possible to assess the success of the refinement and serve as parameters for comparing results are: R_{WP}, which is given in percentage and represents the error associated with each intensity as a function of the number of counts, common values for the R_{WP} are 2% to 20%; R_{EXP}, also given as a percentage, represents the expected statistical error at each intensity; and χ^2, which represents the goodness of fit and determines the convergence of the refinement, with a perfect convergence when $\chi^2 = 1.0$.

Structure refinement using the RM was conducted with the GSAS (General Structure Analysis System) software, available by Larson and Von Dreele[44]. Divergence and reception slits of 0.5º, scanning speed of 0.2º/min and angular range 2θ from 20º to 110º were used. The Crystallographic Information Framework (CIF) files from the Crystallography Open Database (COD) were used as refinement control files.

3.4. Crystallization Kinetics

Kissinger's Method (KM)[45,46] was used to calculate the activation energies of the crystalline phases identified in the glass-ceramics. This method is based on the thermal analysis data of the investigated samples and is one of the most used methods for the study of crystallization kinetics. Although it needs corrections for more complex systems and conditions[47], it is sufficient for activation energy assignments of relatively simple systems such as $CaO\text{-}TiO_2\text{-}SiO_2\text{-}Al_2O_3$. The KM is based on Equation 1 used for the construction of the Kissinger plots.

$$ln\left(\frac{\beta}{T_p^{\,2}}\right) = ln\left(\frac{AR}{E_a}\right) - \frac{E_a}{RT_p} \quad (1)$$

Where β is the heating rate (Ks^{-1}), T_p the absolute temperature of the crystallization peak at each heating rate (K), A the Arrhenius pre-exponential factor (s^{-1}), R the universal gas constant (8.3145 $Jmol^{-1}K^{-1}$), and E_a the activation energy of the crystallized phase ($Jmol^{-1}$). The E_a values can be determined using the $\ln(\beta/T_p^{\,2})$ versus $1/T_p$ plot, resulting in a line equation with $-E_a/R$ as angular coefficient and $\ln(AR/T_p)$ as linear coefficient[48].

The crystallization temperatures for each phase in each of the heating rates (10, 15, 20, 25, and 30 ºC/min) of the three glass-ceramic samples were determined by deconvolution of the respective crystallization peaks (heat flow curves) using the Voigt probabilistic distribution (PeakFit™ software, version 4).

4. Results and Discussion

Figure 1 shows the XRD patterns of the Ca Glass sample. The broadband located around 25º is characteristic of non-crystalline materials (without long-range order), which confirms the material's production in its glassy phase.

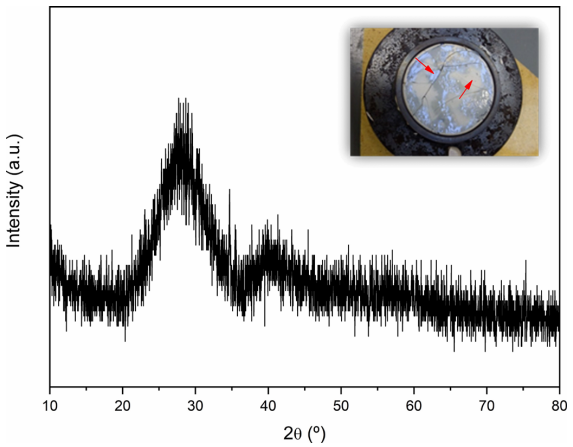

Figure 1. XRD patterns of the Ca Glass. Inset: Photograph of Ca Glass still in the metal mold where it was poured. The arrows point to two apparently distinct regions.

The inset in Figure 1 shows an image of Ca Glass still in the metallic mold after the sample has cooled. It has an opaque appearance, and two regions can be identified, one lighter and the other darker (both indicated by red arrows). The light regions are probably related to the areas where there was a greater diffusion of Al from the crucible to the melted precursors, which usually occurs at temperatures above 1500 ºC[49].

Table 1 shows the semi-quantitative chemical analysis of Ca Glass via XRF spectrometry to confirm the formulation of the produced glass. It is possible to observe that the percentages of the glass constituent oxides are very close to the percentages of the proposed formulation ($CaCO_3$ 47.50 wt%, TiO_2 23.75 wt%, SiO_2 23.75 wt%, and Al_2O_3 5.00 wt%), with the presence of 46.234 wt% of CaO, 22.853 wt% of SiO_2, 22.225 wt% of TiO_2, 8.034 wt% of Al_2O_3, and 0.564 wt% of other oxides (contaminants). The increase in the amount of Al and the decrease in Ca, Si, and Ti in relation to the formulation, are probably explained by the aforementioned diffusion process involving the high-density Al_2O_3 crucible and the melted precursors. There is a minimum concentration of contaminating oxides, and the elemental attribution of Ca is linked to the presence of CaO because of the decomposition $CaCO_3 \rightarrow CaO + CO_2$ (around 740 ºC[50,51]) during the fusion of the precursors.

Ca Glass was also subjected to thermal analysis up to 1300 ºC, at a heating rate of 10 ºC/min (Figure 2), to determine the crystallization peaks (in order to define the heat treatment temperature for the production of glass-ceramic materials). It is possible to observe only two considerable variations in the heat flow. The first is the endothermic reaction around 40 ºC, related to the desorption of water on the vitreous material's surface. The other refers to the exothermic reaction at 900 ºC, related to the glass crystallization (T_p). A definite separation at the crystallization peak was not observed, which suggests that either only one phase was crystallized or the crystallized phases' activation energies were similar in this heating rate[52]. This crystallization peak at 900 ºC is in the temperature range of the titanate perovskite glasses crystallization (730 ºC to 1000 ºC), as verified for the SrO-TiO_2-SiO_2-B_2O_3-La_2O_3[53], SrO-TiO_2-SiO_2-B_2O_3-Bi_2O_3[54], SrO-TiO-SiO_2-B_2O_3-CoO[55], and SrO-TiO_2-SiO_2-B_2O_3-K_2O[56] systems. Therefore, an arbitrary temperature was set just above this crystallization peak, and the Ca Glass was subsequently treated at 960 ºC for the glass-ceramics production.

The XRD patterns for glass-ceramic samples obtained from Ca Glass treated at 960 ºC for 2, 4, and 6 hs are shown in Figure 3a, 3b, and 3c, respectively. All samples present the well-crystallized orthorhombic $CaTiO_3$ (Calcium Titanate) (PDF 22-153) phase, identified by the characteristic peaks around 33º, 48º, 59º, 69º, and 79º. The monoclinic $CaTiSiO_5$ (Titanite) phase (PDF 25-177) patterns also appeared in all samples, but with less intensity than $CaTiO_3$. The patterns of the monoclinic $CaSiO_3$ (Wollastonite) (PDF 72-2297) and orthorhombic $Ca_8Si_5O_{18}$ (Calcium Silicate) (PDF 29-368) phases are very similar. However, the $CaSiO_3$ phase is only present in the 2 hs treated sample (Figure 3a) and is replaced by the $Ca_8Si_5O_{18}$ phase in the 4 and 6 hs treated samples (Figure 3b and 3c, respectively). The main difference between these two phases is observed at the peak around 30º, which is relatively intense in the 2 hs treated sample and characterizes

Table 1. Results of semi-quantitative chemical analysis (wt%) of Ca Glass by XRF spectrometry.

Oxide	Proposed Composition (wt%)	Observed Percentage (wt%)	Line
CaO	47.500	46.324	Ca K_α
SiO_2	23.750	22.853	Si K_α
TiO_2	23.750	22.225	Ti K_α
Al_2O_3	0.500	8.034	Al K_α
SO_3	-	0.339	S K_α
SrO	-	0.082	Sr K_α
K_2O	-	0.070	K K_α
Fe_2O_3	-	0.028	Fe K_α
Co_2O_3	-	0.022	Co K_α
CuO	-	0.012	Cu K_α
ZrO_2	-	0.009	Zr K_α
NbO	-	0.002	Nb K_α

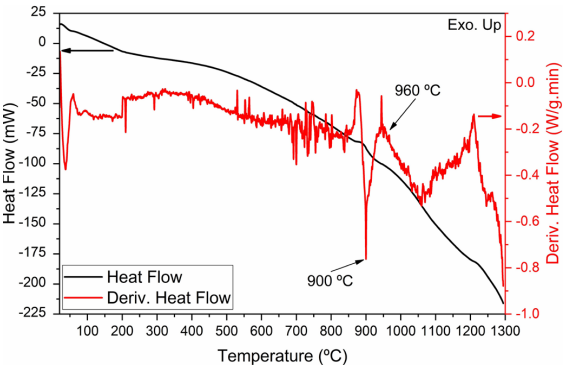

Figure 2. Differential scanning calorimetry of Ca Glass (10 ºC/min heating rate).

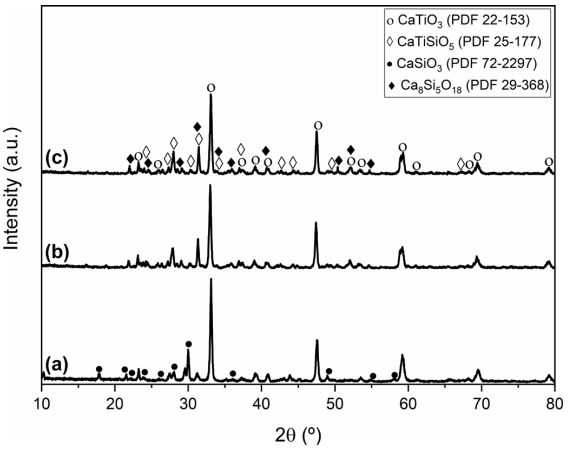

Figure 3. XRD patterns of glass-ceramics obtained from Ca Glass treated at 960 ºC during (a) 2 hs, (b) 4 hs and (c) 6 hs. Assignments: ○ orthorhombic $CaTiO_3$, ◊ monoclinic $CaTiSiO_5$, ● monoclinic $CaSiO_3$ e ♦ orthorhombic $Ca_8Si_5O_{18}$.

the $CaSiO_3$ phase. Kubo et al.[38] identified the existence of similar phases ($CaTiO_3$, $CaTiSiO_5$, Ca_2SiO_3), however for samples produced from the $CaTiO_3$ 20 wt%-$CaSiO_3$ 80 wt% system, treated at 1200 ºC at high pressures (10 to 12 GPa).

As expected for the CaO-TiO_2-SiO_2-Al_2O_3 system, the non-crystalline portion of the samples presented here is practically absent. The verification of this amorphous portion can be done indirectly from the microstructure analysis of the glass-ceramic.

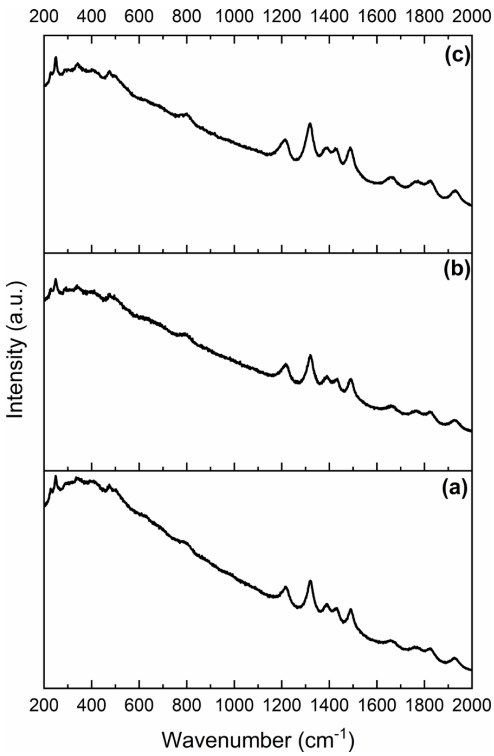

Figure 4. Raman scattering of glass-ceramics obtained from Ca Glass treated at 960 ºC during (a) 2 hs, (b) 4 hs and (c) 6 hs.

The glass-ceramic samples were subjected to Raman scattering to complement the structural characterization, and Figure 4 summarizes the results. The spectra obtained are virtually the same, indicating equivalence of the short-range order for the three samples analyzed. The vibrational modes observed from 200 to 800 cm^{-1} can be attributed to the orthorhombic $CaTiO_3$. They are characterized by the O–Ti–O bonds flexion (at 249, 290 and 339 cm^{-1}), by the Ti–O torsional mode (472 and 500 cm^{-1}), and also by the symmetric elongation of the Ti–O bond (around 800 cm^{-1}), as reported by Cavalcante et al.[57] from the study of $CaTiO_3$ processed in different furnaces. Some of these vibrations overlap with the $CaTiSiO_5$[58] phase modes, which results in broadening of the observed bands. Above 1000 cm^{-1}, the vibration modes that characterize the SiO_4 and CaO_6 clusters are observed, indicating the presence of both $CaSiO_3$ and $Ca_8Si_5O_{18}$[59] structures.

The structure refinement using the RM was performed on the glass-ceramic samples (Figure 5), aiming at a quantitative analysis of the crystalline phases. Table 2 summarizes the results with the percentages of the phases and the convergence parameters. It was possible to verify the coexistence of the orthorhombic $CaTiO_3$ (CIF 2310618), monoclinic $CaTiSiO_5$ (CIF 9000513), and monoclinic $CaSiO_3$ (CIF 9011452) phases for the 2 hs treated sample, and orthorhombic $CaTiO_3$, monoclinic $CaTiSiO_5$, and orthorhombic $Ca_8Si_5O_{18}$ (CIF 9016471), for samples treated during 4 and 6 hs, corroborating with the conventional diffractograms (without refinement). When increasing heat treatment time from 2 to 6 hs, the $CaTiO_3$ portion increases from 62.97 wt% to 79.21 wt%, and the $Ca_8Si_5O_{18}$ phase also increases (0.00 wt% to 9.54 wt%). In both cases, the increase is linked to the titanite portion decrease (32.00 wt% to 11.25 wt%).

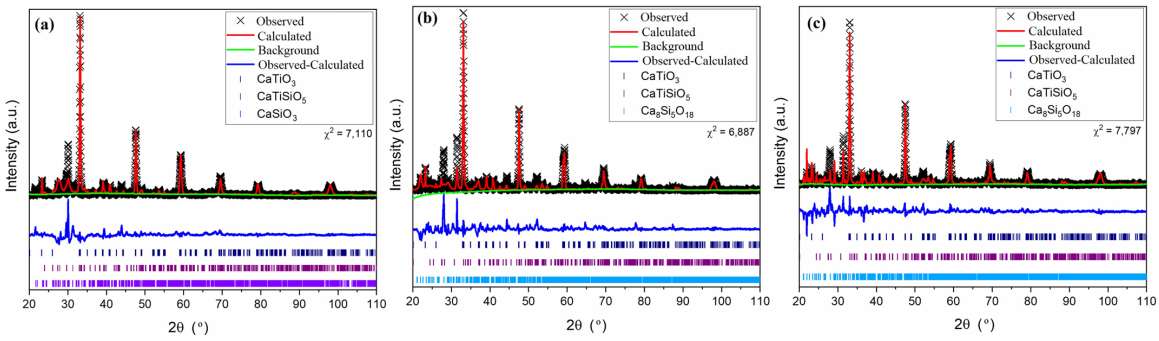

Figure 5. Structure refinement of glass-ceramics obtained from Ca Glass treated at 960 ºC during (a) 2 hs, (b) 4 hs and (c) 6 hs.

Table 2. Phase percentages estimated by the structure refinement for Ca Glass treated at 960 ºC. The convergence parameters are indicated.

Sample	Phase (wt%)				Convergence Parameters		
	$CaTiO_3$ (Calcium Titanate)	$CaTiSiO_5$ (Titanite)	$CaSiO_3$ (Wollastonite)	$Ca_8Si_5O_{18}$ (Calcium Silicate)	R_{WP} (%)	R_{EXP} (%)	χ^2
960 ºC 2 hours	62.97	32.00	5.03	-	14.74	5.53	7.110
960 ºC 4 hours	71.12	23.21	-	5.67	13.07	4.98	6.887
960 ºC 6 hours	79.21	11.25	-	9.54	14.63	5.24	7.797

The narrow stoichiometry that defines titanite justifies its instability with heat treatment.

High values for χ^2 (7.110 – 2 hs, 6.887 – 4 hs and 7.797 – 6 hs) are noticed, probably due to two factors: (1) the abnormal high intensity observed for (002) plane of the $CaTiSiO_5$ phase, around 28º (based on the reference CIF 9000513 there is a preferential growth of this plane in the produced glass-ceramics), and (2) the persistence of the amorphous phase in smaller portions, which is indicated by the background flexion (Figure 5), hindering the convergence during refinement[60]. However, the values obtained for χ^2 allow the use of these results as control files.

Therefore, there is glass-ceramic material formation at all times in samples crystallized at 960 ºC. However, the crystalline portions and probably amorphous portions are unstable at this temperature and depend on the heat treatment time.

Figure 6 shows the optical microscopies of the glass-ceramic samples treated in HF solution (microstructures analysis). It is possible to identify two distinct regions for all samples, a lighter one consisting of cross-like structures, referring to the attacked crystalline portion, and a darker one referring to the vitreous matrix. The different orientations for the observed patterns are probably linked to the grains' different orientations (polycrystalline phases). For the 2 hs heat-treated sample (Figure 6a and 6a'), it is possible to observe lighter regions (white arrows), probably related to the segregation of the wollastonite phase[61]. The 4 hs (Figure 6b and 6b') and 6 hs (Figures 6c and 6c') samples are more similar to each other. It is possible to observe the growth of the cross-like structures for the 6 hs sample, which may be related to grain growth.

EDS analysis (Figure 7) was carried out for the glass-ceramic sample, which was heat-treated for 6 hs and attacked in an acid solution. Three distinct regions were analyzed (spectrum 1, 2, and 3). As expected, the elements Ca, Si, Ti, Al, O, and Au (metallization) were identified. It is important to note that Al is present both in the vitreous matrix and in the crystalline phases (cross-like microstructures), even though there is no crystallization of any phase that has Al. Also, the concentration of this element is higher in the vitreous phase (spectrum 1). The non-crystalline portion has a low Ti concentration, most likely due to the already mentioned rapid crystallization of the $CaTiO_3$ phase.

From the EDS analysis of the glass-ceramics without attack in acid solution and at a greater magnification (Figure 8), it is

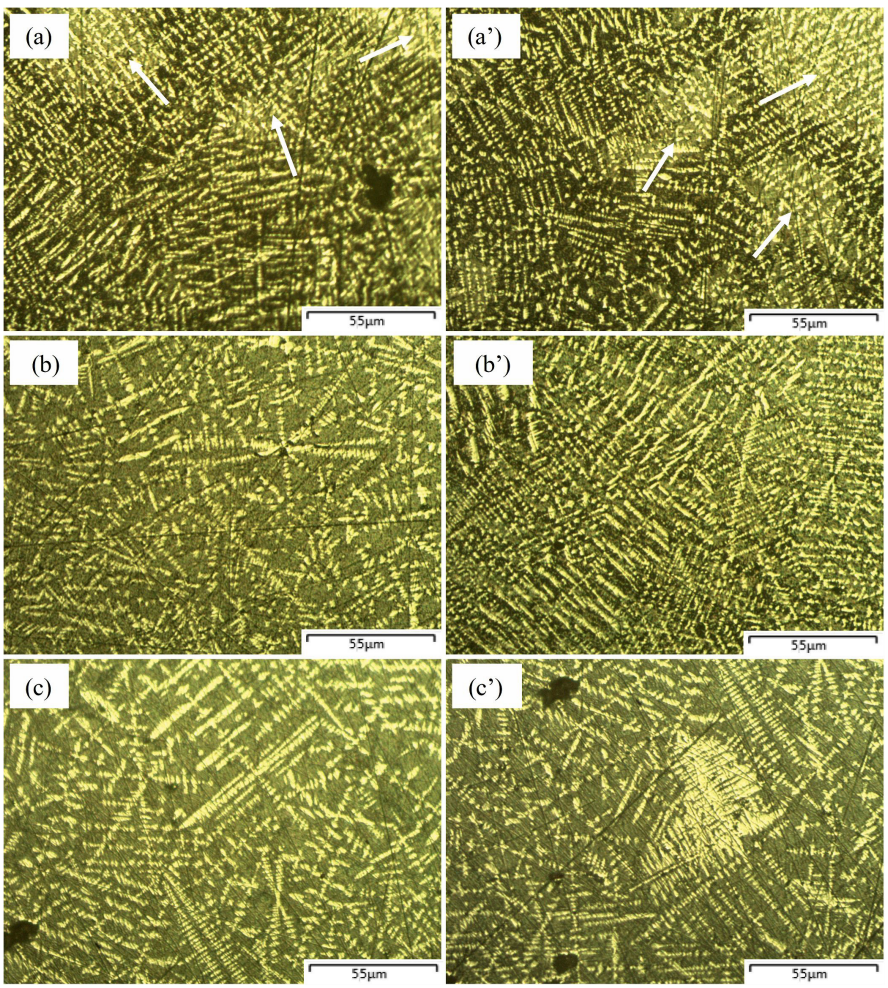

Figure 6. Optical microscopies of glass-ceramics obtained from Ca Glass treated at 960 ºC during (a), (a ') 2 hs, (b), (b'), 4 hs and (c), (c ') 6 hs. Samples treated in HF solution.

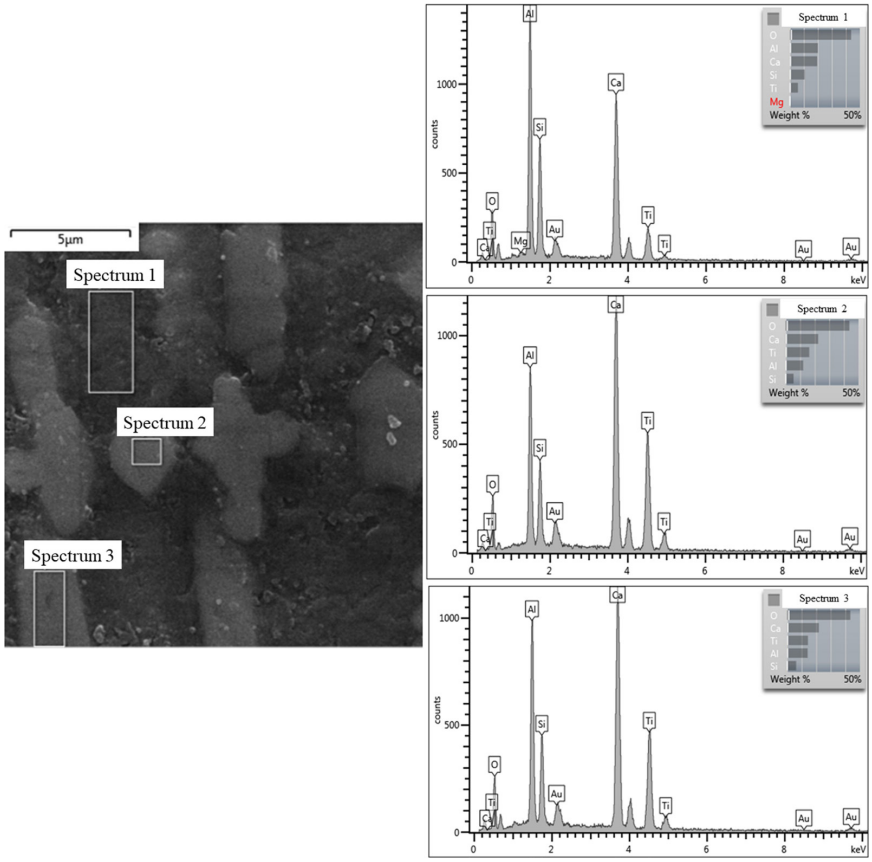

Figure 7. SEM and EDS analyses of glass-ceramic obtained from Ca Glass treated at 960 ºC during 6 hs. Three different regions were analyzed (spectrum 1, 2 and 3).

possible to notice a homogeneous distribution of the Ca, Si, and Ti elements only for the 2 hs treated sample. Apparently, there is gradual segregation of the $CaTiO_3$ phase as the heat treatment time increases, as evidenced by Figures 8b and 8c – higher concentration of Ca and Ti in some regions, which can also be noticed by the microstructure analyzed in Figure 6c' – high concentration of cross-like structures in a single region. The rapid crystallization and consequent microstructural segregation of the $CaTiO_3$ phase are probably linked to the low activation energy for this phase's crystallization. For example, in $CaTiO_3$ bulk crystallization by the hydrothermal method, the activation energy is only 89 kJ/mol[62].

Ca Glass was again subjected to thermal analysis under different heating rates (10, 15, 20, 25, and 30 ºC/min – Figure 9) in order to carry out the kinetic studies. As expected, as the heating rate increases, the crystallization peak shifts to higher temperatures and widens[63], suggesting greater separation between the crystallization peaks of the individual phases. The center of this crystallization peak at 900 ºC (10 ºC/min) shifts to 925 ºC (15 ºC/min), 930 ºC (20 ºC/min), 935 ºC (25 ºC/min), and 952 ºC (30 ºC/min). From the deconvolution of these peaks (Figure 10), it was possible to determine the crystallization temperature of each of the three phases (curves 1, 2, and 3, referring to phases 1, 2, and 3, respectively) for each of the heating rates. Based on these results, it was possible to estimate each phase's activation energy by constructing the Kissinger plots (Figure 11).

Table 3. Activation energies obtained by the Kissinger Method for Phase 1 (Curve 1), Phase 2 (Curve 2) and Phase 3 (Curve 3), crystallized after the heat treatment of Ca Glass.

Phase	Activation Energy (kJ/mol)	Assignment
1	217 ± 10	$CaTiO_3$
2	281 ± 08	$CaSiO_3$
3	446 ± 20	$CaTiSiO_5$
Average	315 ± 13	-

The deconvolution was carried out in three phases, as this is the number of crystalline phases identified by the structural characterizations, and this number of curves was the one that resulted in the best fit (the smallest difference between the observed and calculated curves).

The Kissinger plots showed excellent linear adjustments and allowed the calculation of the activation energies (Table 3) for curves 1, 2, and 3 (phases 1, 2, and 3). These energies can be attributed to the crystalline phases identified by XRD. Phase 1, which has activation energy around 217 kJ/mol, is the lowest value found and can be attributed to the $CaTiO_3$ phase (rapid crystallization). Phase 2 presents activation energy around 281 kJ/mol, a value very close to the activation energy of glass-ceramics with

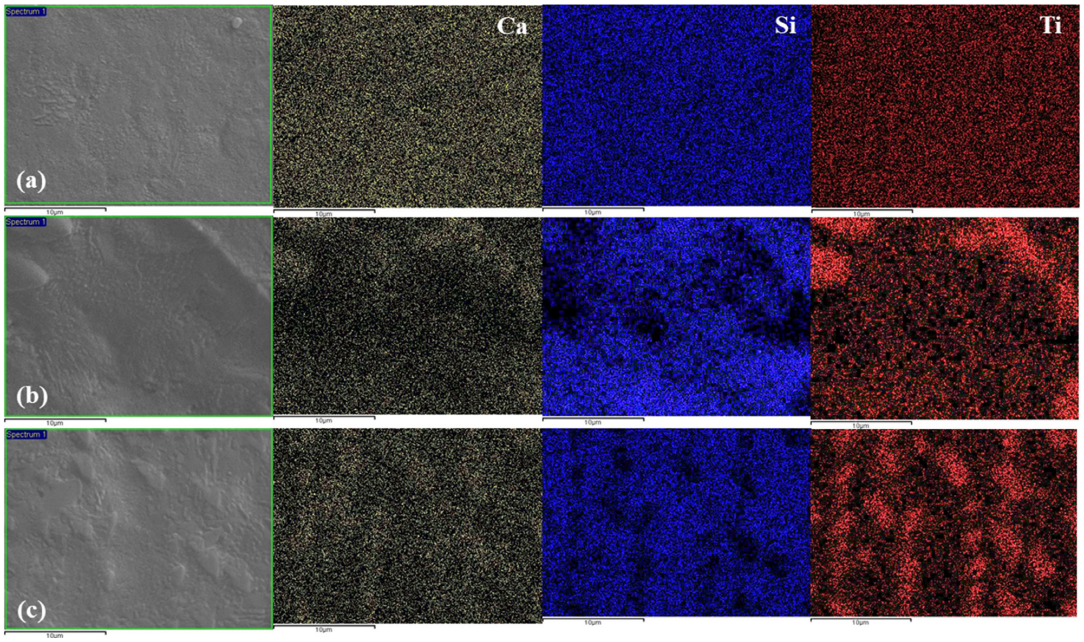

Figure 8. SEM and EDS analyses of glass-ceramics obtained from Ca Glass treated at 960 ºC during (a) 2 hs, (b) 4 hs and (c) 6 hs. Reference bars: 10 µm.

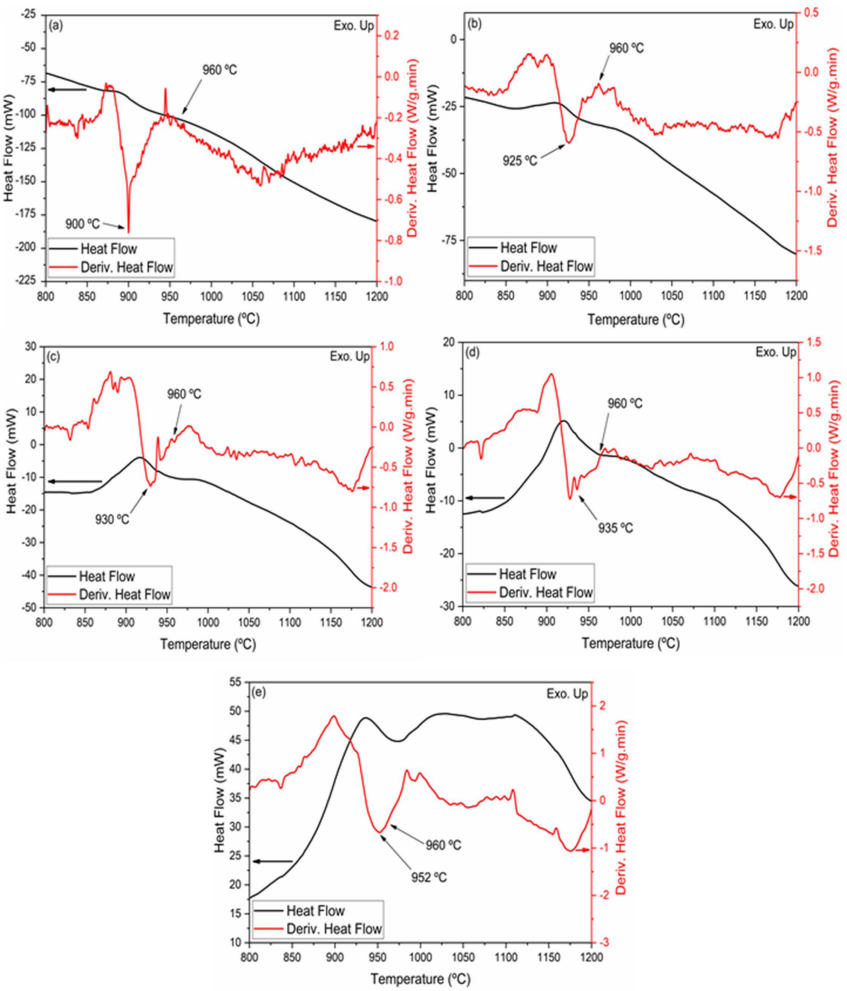

Figure 9. Differential scanning calorimetry of Ca Glass. Heating rate of (a) 10 ºC/min, (b) 15 ºC/min, (c) 20 ºC/min, (d) 25 ºC/min and (e) 30 ºC/min.

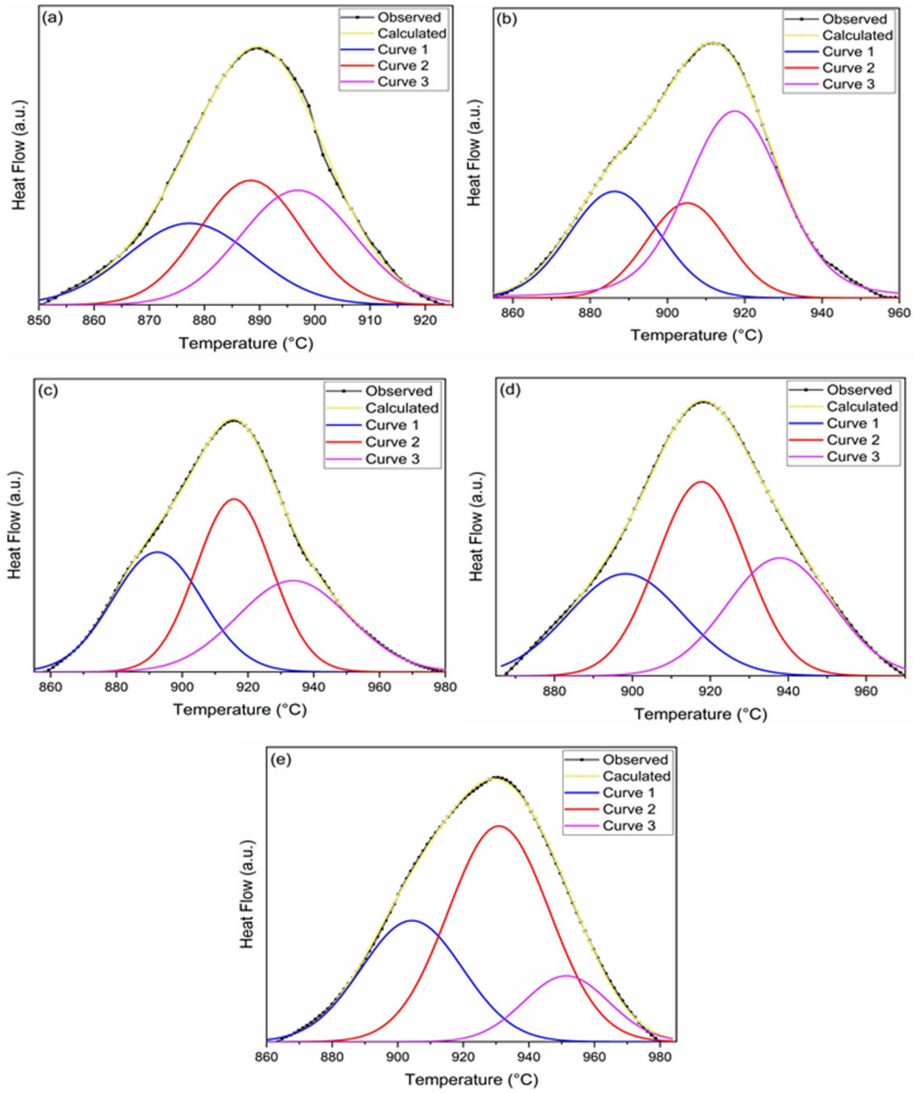

Figure 10. Deconvolution of the Ca Glass crystallization peaks. Heating rate of (a) 10 ºC/min, (b) 15 ºC/min, (c) 20 ºC/min, (d) 25 ºC/min and (e) 30 ºC/min.

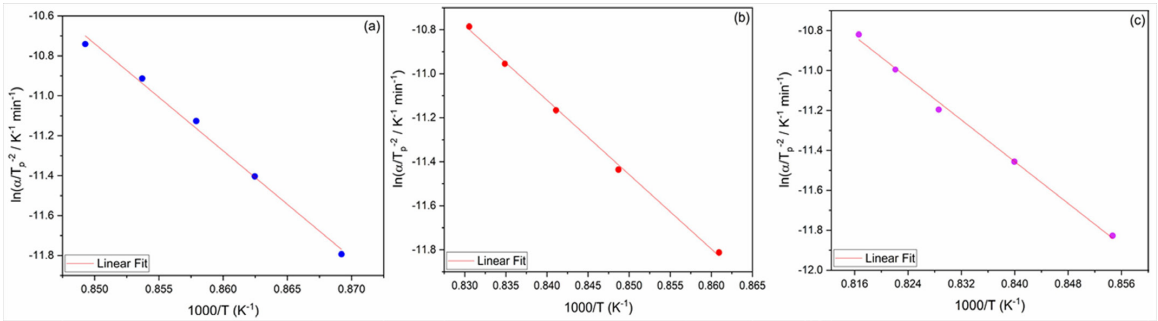

Figure 11. Kissinger plots: Determination of the activation energies obtained from the crystallization peak in Ca Glass. (a) Curve 1, (b) Curve 2 and (c) Curve 3.

wollastonite as the main phase (~ 262 kJ/mol calculated by KM[64]). It was not possible to find values for the activation energy of glass-ceramics with the $CaTiSiO_5$ phase. However, according to the reported high theoretical enthalpy of formation of this phase (~ 2601 kJ/mol[65]), it is possible to assign the calculated energy for Phase 3, 446 kJ/mol, to $CaTiSiO_5$. Therefore, from the KM, it is concluded that the average activation energy for obtaining the glass-ceramics (CaO 47.50 wt%-TiO_2 23.75 wt%-SiO_2 23.75 wt%-Al_2O_3 5.00 wt% system) is approximately 315 kJ/mol.

5. Conclusions

Glass samples of the CaO 47.50 wt%-TiO_2 23.75 wt%-SiO_2 23.75-Al_2O_3 5.00 wt% system were obtained by the melt-quenching technique (1650 ºC). There was a small deviation from the proposed formulation due to diffusion of Al from the crucible to the melted precursors: CaO 46.234 wt%-TiO_2 22.225 wt%-SiO_2 22.853-Al_2O_3 8.034 wt%-contaminants 0.564 wt%. Glass-ceramics were obtained from the treatment of these glasses at 960 ºC during 2, 4, and 6 hs. The phases $CaTiO_3$, $CaSiO_3$ (only in the 2 hs treated sample), $Ca_8Si_5O_{18,}$ and $CaTiSiO_5$ were identified.

Structure refinement using the Rietveld method showed that the secondary phases ($CaSiO_3$ and $CaTiSiO_5$) are metastable and that there is an increase in the percentage of the other phases $CaTiO_3$ (62.97 wt% to 79.21 wt%) and $Ca_8Si_5O_{18}$ (0.00 wt% to 9.54 wt%) as the heat treatment time increases. From the EDS and microstructure analysis, it was possible to identify cross-like structures forming a crystallized net embedded in a non-crystallized phase, with Ti deficiency.

The crystallization kinetics by the Kissinger method allowed identify the activation energies of the crystallized phases from the proposed glass's thermal treatment, with the values of 217, 281, and 446 kJ/mol for the $CaTiO_3$, $CaSiO_{3,}$ and $CaTiSiO_5$ phases, respectively. The structural, microstructural, and kinetics studies for this type of glass-ceramic material are rarely addressed in the literature. Therefore, these data can serve as a reference for future research involving glass-ceramic perovskites with potential electronic applications, such as the $CaTiO_3$ glass-ceramic.

6. Acknowledgements

This study was financed in part by the CDMF/FAPESP 2013/07296-2 - CEPID and by Coordenação de Aperfeiçoamento de Pessoal de Nível Superior - Brasil (CAPES) - Finance Code 001.

We would like to thanks to Ildikó Pete for the valuable discussion.

We would like to thanks São Paulo State Public Ministry and Federal Public Ministry for the LCGRS implementation – Laboratório de Caracterização e Gestão de Resíduos Sólidos [Solid Waste Characterization and Management Laboratory], where this work was developed.

7. References

1. Deubener J, Allix M, Davis MJ, Duran A, Höche T, Honma T, et al. Updated definition of glass-ceramics. J Non-Cryst Solids. 2018;501:3-10.
2. Zanotto ED. A bright future for glass-ceramics - from their glorious past, starting with their accidental discovery, to successful commercial products, the impressive range of properties and exciting potential applications of glass-ceramics indeed ensure a bright future! Am Ceram Soc Bull. 2010;89(8):19-27.
3. Pannhorst W. Glass ceramics: state-of-the-art. J Non-Cryst Solids. 1997;219:198-204.
4. Marangoni M, Nait-Ali B, Smith DS, Binhussain M, Colombo P, Bernardo E. White sintered glass-ceramic tiles with improved thermal insulation properties for building applications. J Eur Ceram Soc. 2017;37:1117-25.
5. Teixeira SR, Souza AE, Carvalho CL, Reynoso FCS, Romero M, Rincón JM. Characterization of a wollastonite glass-ceramic material prepared using sugar cane bagasse ash (SCBA) as one of the raw materials. Mater Charact. 2014;98:209-14.
6. Zhang M, Pu X, Chen X, Yin G. In-vivo performance of plasma-sprayed CaO–MgO–SiO_2-based bioactive glass-ceramic coating on Ti–6Al–4V alloy for bone regeneration. Heliyon. 2019;5:e02824.
7. Haftbaradaran-Esfahani M, Ahmadian M, Nassajpour-Esfahani AH. Fabrication and characterization of porous biomedical Vitallium alloy with 58S bioglass coating prepared by sol-gel method. Appl Surf Sci. 2020;506:144959.
8. Tran TNL, Armellini C, Varas S, Carpentiero A, Chiappini A, Gluchowski P, et al. Assessment of SnO_2-nanocrystal-based luminescent glass-ceramic waveguides for integrated photonics. Ceram Int. 2021;47(4):5534-41.
9. Biskri ZE, Rached H, Bouchear M, Rached D. Computational study of structural, elastic and electronic properties of lithium disilicate ($Li_2Si_2O_5$) glass-ceramic. J Mech Behav Biomed Mater. 2014;32:345-50.
10. Du X, Pu Y, Li X, Peng X, Sun Z, Zhang J, et al. Optimizing the energy storage performance of K_2O-Nb_2O_5-SiO_2 based glass-ceramics with excellent temperature stability. Ceram Int. 2021;47(7):8987-95.
11. Yadav AK, Gautam CR. A review on crystallisation behaviour of perovskite glass ceramics. Adv Appl Ceramics. 2014;113(4):193-207.
12. Tyurnina ZG, Tyurnina N, Sviridov SI, Sinelshchikova OY, Tumarkin AV, Drozdovsky AV, et al. Formation of new glass-ceramic materials with controllable dielectric and magnetic properties. Key Eng Mater. 2019;822:856-63.
13. Liu S, Shen B, Hao H, Zhai J. Glass–ceramic dielectric materials with high energy density and ultra-fast discharge speed for high power energy storage applications. J Mater Chem C Mater Opt Electron Devices. 2019;7:15118-35.
14. Renka S, Klaser T, Burazer S, Mosner P, Kalenda P, Santic A, et al. High electronically conductive tungsten phosphate glass-ceramics. Nanomaterials. 2020;10:2515-27.
15. Herczog A. Microcrystalline $BaTiO_3$ by crystallization from glass. J Am Ceram Soc. 1964;47:107-15.
16. Kokubo T, Kung C, Tashiro M. Crystallization process of a BaO•TiO_2-A_2O_3-SiO_2 glass. Yogyo Kyokaishi. 1969;77:367-71.
17. Yao K, Zhang L, Yao X, Zhu W. Preparation and properties of barium titanate glass–ceramics sintered from sol-gel powders. J Mater Sci. 1997;32:3659-65.
18. McCauley D, Newnham RE, Randall CA. Intrinsic size effects in a $BaTiO_3$ glass ceramic. J Am Ceram Soc. 1998;81:979-87.
19. Yadav P, Sagdeo A, Sinha A, Laila NP. Rubbing induced strain-glass phase on ceramic $BaTiO_3$ surface. Ceram Int. 2019;45(15):19044-8.
20. Ramoska T, Banys J, Sobiestianskas R, Petrovic MV, Bobic J, Stojanovic B. Dielectric investigations of La-doped barium titanate. Process Appl Ceram. 2010;4:193-8.
21. Kokubo T. Preparation and properties of glass-ceramics containing ferroelectric crystals. Bull Inst Chem Res Kyoto Univ. 1969;47(6):553-71.
22. Swartz SL, Bhalla AS, Cross LE. Low-temperature dielectric properties of $SrTiO_3$ glass-ceramics. J Appl Phys. 1986;60:2069-81.
23. Saegusa K. $PbTiO_3$-PbO-B_2O_3 glass ceramics by a sol gel process. J Am Ceram Soc. 1996;79:3282-8.
24. Salami TJ, Imanieh SH, Lawrence JG, Martin IR. Amorphous glass-perovskite composite as solid electrolyte for lithium-ion battery. Mater Lett. 2019;254(1):294-6.
25. Wang X, Wang P, Zhao H, Tian K, Jia S, Wang S, et al. Ultra-broadband near-infrared photoluminescence in Er^{3+}-Ni^{2+} co-doped transparent glass ceramics containing nano-perovskite $KZnF_3$. Ceram Int. 2020;46(16):25987-91.

26. Sarakha L, Bousquet A, Tomasella E, Boutinaud P, Mahiou R. Investigation of $CaTiO_3:Pr^{3+}$ thin films deposited by radiofrequency reactive magnetron sputtering for electroluminescence application. IOP Conf Series Mater Sci Eng. 2009;12:012008.
27. Lu X, Li Q, Yang D. Dielectric properties and sintering characteristics of $CaTiO_3$-$(Li_{1/2}Nd_{1/2})TiO_3$ ceramics. J Electroceram. 2005;14:59-65.
28. Perrella RV, Ribeiro IC, Campos-Junior PHA, Schiavon MA, Pecoraro E, Ribeiro SJL. $CaTiO_3:Er^{3+}:Yb^{3+}$ upconversion from 980 nm to 1550 nm excitation and its potential as cells luminescent probes. Mater Chem Phys. 2019;223:391-7.
29. Wiff JP, Fuenzalida VM, Zárate RA, Arias JL, Fernández MS. Characterization of hydrothermal–electrochemical calcium titanate coatings on titanium and biomedical titanium alloy. J Phys Condens Matter. 2004;16(14):S1345.
30. Shimura K, Yoshida H. Hydrogen production from water and methane over Pt-loaded calcium titanate photocatalyst. Energy Environ Sci. 2010;3:615-7.
31. Jiang Z, Han J, Liu X. Immobilization of radioactive wastes into $CaTiO_3$ synroc by the SHS method. Adv Mat Res. 2010;152-153:315-9.
32. Sanoj MA, Varma MR. Sinterability and microwave dielectric properties of $0.95MgTiO_3$–$0.05CaTiO_3$–glass ceramic composites. J Alloys Compd. 2009;477:565-9.
33. Ren L, Luo X, Hu L, Sun Q, Xia Y, Hu Y, et al. Synthesis and characterization of LTCC compositions with middle permittivity based on CaO-B_2O_3-SiO_2 glass/$CaTiO_3$ system. J Eur Ceram Soc. 2017;37(2):619-23.
34. Gautam CR, Das S, Gautam SS, Madheshiya A, Singh AK. Processing and optical characterization of lead calcium titanate borosilicate glass doped with germanium. J Phys Chem Solids. 2018;115:180-6.
35. Almasri KA, Sidek HAA, Matori KA, Zaid MHM. Effect of sintering temperature on physical, structural and optical properties of wollastonite based glass-ceramic derived from waste soda lime silica glasses. Results Phys. 2017;7:2242-7.
36. Francis AA, Rahman MKA. Manufacturing of wollastonite-based glass from cement dust: physical and mechanical properties. Cogent Eng. 2016;3(1):1170750.
37. Soares VO, Daguano JKMB, Lombello CB, Bianchin OS, Gonçalves LMG, Zanotto ED. New sintered wollastonite glass-ceramic for biomedical applications. Ceram Int. 2018;44(16):20019-27.
38. Kubo A, Suzuki T, Akaogi M. High pressure phase equilibria in the system $CaTiO_3$-$CaSiO_3$: stability of perovskite solid solutions. Phys Chem Miner. 1997;24:488-94.
39. DeVries RC, Roy R, Osborn EF. Phase equilibria in the system CaO-TiO_2-SiO_2. J Am Ceram Soc. 1955;38:158-71.
40. Danek V, Nerád I. Phase diagram and structure of melts of the system CaO-TiO_2-SiO_2. Chem Pap. 2002;56(4):241-6.
41. Salinga M, Carria E, Kaldenbach A, Bornhöfft M, Benke J, Mayer J, et al. Measurement of crystal growth velocity in a melt-quenched phase-change material. Nat Commun. 2013;4:2371.
42. Rietveld HM. A profile refinement method for nuclear and magnetic structures. J Appl Cryst. 1969;2:65-71.
43. Kinast EJ. Refinamento estrutural com o método rietveld: implementação e ensaios com o programa fullprof [Structural refinement with the rietveld method: implementation and testing with the fullprof software] [dissertation]. Porto Alegre: Universidade Federal do Rio Grande do Sul; 2000.
44. Larson AC, Von Dreele RB. General structure analysis system (GSAS) program. Los Alamos, NM: Los Alamos National Laboratory, University of California; 2004. (Rep. Nº. LAUR; 86-748).
45. Kissinger HE. Variation of peak temperature with heating rate in differential thermal analysis. J Res Natl Bur Stand. 1956;57(4):217-21.
46. Kissinger HE. Reaction kinetics in differential thermal analysis. Anal Chem. 1957;29(11):1702-6.
47. Vyazovkin S. Kissinger method in kinetics of materials: things to beware and be aware of. Molecules. 2020;25:2813.
48. Silva G, Nakamura NM, Iha K. Kinetic study of the thermal decomposition of pentaerythritol-tetranitrate (PETN). Quim Nova. 2008;31(8):2060-4.
49. Barz A, Haase T, Meyer K, Stachel D. Corrosion of crucible materials and their influence on structure of phsophate glasses. Phosphorus Res Bull. 1995;6:331-5.
50. Narsimhan G. Thermal decomposition of calcium carbonate. Chem Eng Sci. 1961;16(1-2):7-20.
51. Mohamad SFS, Mohamad S, Jeemat Z. Study of calcination condition on the composition of calcium carbonate in waste cockle shell to calcium oxide usingthermal gravimetric analysis. J Eng Appl Sci. 2016;11:9917-21.
52. Zheng Q, Zhang Y, Montazerian M, Gulbiten O, Mauro JC, Zanotto ED, et al. Understanding glass through differential scanning calorimetry. Chem Rev. 2019;119(13):7848-939.
53. Thakur OP, Kumar D, Parkash O, Pandey L. Crystallization and microstructural behaviour of strontium titanate borosilicate glass ceramics with Bi_2O_3 addition. Bull Mater Sci. 1997;20:67-77.
54. Thakur OP, Kumar D, Parkash O, Pandey L. Dielectric behaviour of strontium titanate glass ceramics with bismuth oxide addition as nucleating agent. Indian Journal of Physics A. 1997;71:161-72.
55. Thakur OP, Kumar D, Parkash O, Pandey L. Effect of K_2O addition on crystallization and microstructural behavior of strontium titanate borosilicate glass ceramic system. Mater Lett. 1995;23:253-60.
56. Thakur OP, Kumar D, Parkash O, Pandey L. Incommensurate crystal growth behaviour in strontium titanate glass ceramic system. Mod Phys Lett B. 2002;16:1037-47.
57. Cavalcante LS, Marques VS, Sczancoski JC, Escote MT, Joya MR, Varela JA, et al. Synthesis, structural refinement and optical behavior of $CaTiO_3$ powders: a comparative study of processing in different furnaces. Chem Eng J. 2008;143(1-3):299-307.
58. Zhang M, Salje EKH, Redfern SAT, Bismayer U, Groat LA. Intermediate structures in radiation damaged titanite ($CaTiSiO_5$): a Raman spectroscopic study. J Phys Condens Matter. 2013;25:115402.
59. Mihailova B, Konstantinov L, Dinolova E. Cluster-approximation modelling of infrared and Raman spectra of crystalline and vitreous $CaSiO_3$. J Non-Cryst Solids. 1995;191(1-2):79-84.
60. De La Torre AG, Bruque S, Aranda MAG. Rietveld quantitative amorphous content analysis. J Appl Cryst. 2001;34:196-202.
61. Yao SY, Cao HX, Wang P, Zhang WW, Huo WL, Xu W. Phase transformation and microstructure of wollastonite glass–ceramics in Na_2O–CaO–SiO_2 system under different heat treatment conditions. Mater Res Innov. 2014;18:657-60.
62. Croker D, Loan M, Hodnett BK. Kinetics and mechanisms of the hydrothermal crystallization of calcium titanate species. Cryst Growth Des. 2009;9(5):2207-13.
63. Matos JR, Miyano MH, Siqueira L, Moura MFV, Luiz JM. Ilustração da influência da razão de aquecimento nos resultados de termogravimetria. Quim Nova. 2000;23:113-5.
64. Si W, Ding C. An investigation on crystallization property, thermodynamics and kinetics of wollastonite glass ceramics. J Cent South Univ. 2018;25:1888-94.
65. Tangeman J, Xirouchakis D. High-temperature heat capacity and thermodynamic properties for end-member titanite ($CaTiSiO_5$). Phys Chem Miner. 2001;28:167-76.